THE JOURNAL OF BIOLOGICAL CHEMISTRY VOL. 290, NO. 10, pp. 6010–6021, March 6, 2015

SH2B1 and IRSp53 Proteins Promote the Formation of Dendrites and Dendritic Branches*

Received for publication, August 18, 2014, and in revised form, January 2, 2015 Published, JBC Papers in Press, January 13, 2015, DOI 10.1074/jbc.M114.603795

Chien-Jen Chen[‡1], Chien-Hung Shih[‡1], Yu-Jung Chang[‡1], Shao-Jing Hong[‡], Tian-Neng Li[§], Lily Hui-Ching Wang[§¶], and Linyi Chen[‡¶2]

From the [‡]Institute of Molecular Medicine, [§]Institute of Molecular and Cellular Biology, [¶]Department of Medical Science, National Tsing Hua University, Hsinchu, Taiwan 30013, China

Background: Filopodium formation is a prerequisite for neurite initiation.
Results: SH2B1 interacts with IRSp53 and promotes neurite outgrowth of hippocampal neurons.
Conclusion: SH2B1-IRSp53 complexes promote filopodium formation, neurite initiation, and neurite branching.
Significance: These results suggest that SH2B1 may regulate the formation of filopodia required for many cellular functions.

SH2B1 is an adaptor protein known to enhance neurite outgrowth. In this study, we provide evidence suggesting that the SH2B1 level is increased during *in vitro* culture of hippocampal neurons, and the *β* isoform (SH2B1*β*) is the predominant isoform. The fact that formation of filopodia is prerequisite for neurite initiation suggests that SH2B1 may regulate filopodium formation and thus neurite initiation. To investigate whether SH2B1 may regulate filopodium formation, the effect of SH2B1 and a membrane and actin regulator, IRSp53 (insulin receptor tyrosine kinase substrate p53), is investigated. Overexpressing both SH2B1*β* and IRSp53 significantly enhances filopodium formation, neurite outgrowth, and branching. Both *in vivo* and *in vitro* data show that SH2B1 interacts with IRSp53 in hippocampal neurons. This interaction depends on the N-terminal proline-rich domains of SH2B1. In addition, SH2B1 and IRSp53 co-localize at the plasma membrane, and their levels increase in the Triton X-100-insoluble fraction of developing neurons. These findings suggest that SH2B1-IRSp53 complexes promote the formation of filopodia, neurite initiation, and neuronal branching.

During development, neural stem cells undergo a morphogenetic series to become mature neurons in response to extrinsic as well as intrinsic factors. One prominent feature of neurogenesis is neurite outgrowth. Although an array of studies have identified the growth factors, receptors, and signaling events that are responsible for neurite outgrowth and guidance, intrinsic regulation for neurite initiation is less clear. For hippocampal and cortical neurons cultured *in vitro*, the formation of lamellipodia containing filopodia is required for navigation of neurites. Thus, the coordination of actin and microtubule assembly becomes a major determinant of neurite outgrowth. As several studies have implicated the importance of filopodia in neurite formation, a recent report clearly demonstrates the formation of filopodia preceding neurite initiation (1). Dent *et al.* (1) show that extracellular matrix laminin promotes the formation of actin-rich protrusions (filopodium-like) and is able to rescue neuritogenesis in vasodilator-stimulated phosphoprotein (VASP)[3]-deficient neurons. This study also reveals the importance of regulators of filopodium formation during neurite outgrowth.

Filopodia are actin-rich membrane protrusions involve in cell migration, neurite initiation, axon guidance in neuronal growth cones, endocytosis, and wound healing (1–3). Filopodia consist of unbranched F-actin filament bundles that are regulated by many actin-binding proteins such as IRSp53 (insulin receptor tyrosine kinase substrate p53), fascin, Mena/VASP, and formins (3–5). IRSp53 belongs to Inverse Bin-Amphiphysin-Rvs 167 (I-BAR), also known as IMD (IRSp53-missing in metastasis homology domain), domain-containing superfamily of proteins and is known to drive membrane deformation, the subsequent plasma membrane protrusions, and thus filopodium formation (3, 6–8). They are retracted by retrograde flow of F-actin and capping protein activity. The dynamic balance of barbed-end actin polymerization and retraction determines the initiation, maintenance, and stability of filopodia. The molecular mechanisms for controlling the initiation of dendritic filopodia are not clear.

IRSp53 contains IMD, CRIB (Cdc42/Rac-interactive binding), Src homology 3 (SH3), WW domains, and PDZ domain binding sites (3). The IMD domain allows IRSp53 targeting to plasma membrane by binding to lipid molecules and triggers membrane protrusion (3, 8). The SH3 domain of IRSp53 has been shown to interact with regulatory proteins of actin, allowing IRSp53 to regulate actin cytoskeleton-associated proteins and thus filopodium formation (8). The polymerization state of actin is important in affecting IMD-lipid interaction. Monomeric actin partially disrupts the binding between IMD and lipid, whereas assembled actin filament stabilizes the IRSp53-lipid interaction (9).

* This work was supported by National Science Council of Taiwan Grant NSC101-2311-B-007-012-MY3 and National Health Research Institutes Grant NHRI-EX104-10206NI.
[1] These authors contributed equally to this work.
[2] To whom correspondence should be addressed: Institute of Molecular Medicine and Dept. of Medical Science, National Tsing Hua University, 101, Section 2, Kuang-Fu Rd., Hsinchu, Taiwan 30013, China. Tel.: 886-3-5742775; Fax: 886-3-5715934; E-mail: lchen@life.nthu.edu.tw.

[3] The abbreviations used are: VASP, vasodilator-stimulated phosphoprotein; DIV, day *in vitro*; PLA, proximity ligation assay; SH, Src homology.

SH2B1 belongs to the SH2B adaptor proteins family, including SH2B1 (SH2-B), SH2B2 (APS), and SH2B3 (Lnk) (10–13). Four SH2B1 splice variants identified so far, α, β, γ, and δ, differ only in their C termini (11, 14). SH2B1 contains two proline-rich domains, two actin-binding regions, a pleckstrin homology domain, and an SH2 domain. SH2B1 also has a nuclear localization sequence and a nuclear export sequence, which affect its cellular distribution and thus differentiation genes (15–19). Human subjects with SH2B1 mutations display behavioral abnormalities, including social isolation and aggression (20–22). Overexpressing SH2B1β has previously been shown to enhance neurite outgrowth of neuronal PC12 cells and cortical and hippocampal neurons (18, 19, 23–26). However, exactly how SH2B1 promotes neurite initiation remains unclear. Using the hippocampal and cortical neuron culture, we tested the hypothesis that SH2B1 promotes filopodium formation and thus neurite initiation by interacting with IRSp53.

MATERIALS AND METHODS

Animal Handling and Ethics Statement—All experiments were conducted in accordance with the guidelines of the Laboratory Animal Center of National Tsing Hua University. Animal use protocols were reviewed and approved by the National Tsing Hua University Institutional Animal Care and Use Committee (approval number 10126).

Antibodies and Reagents—Polyclonal antibody to rat SH2B1 was raised against a glutathione *S*-transferase fusion protein containing amino acids 527–670 of SH2B1β, as described previously (27), and was used at a dilution of 1:1000 for Western blotting. Anti-IRSp53, used at a dilution of 1:5000 for Western blotting and 1:200 for immunoprecipitation, and anti-Myc antibodies, used at a dilution of 1:1000 for Western blotting and 1:200 for immunoprecipitation, were purchased from Millipore (Billerica, MA). Anti-MAP2 (used at a dilution of 1:200 for immunostaining), anti-Tau-1 (used at a dilution of 1:200 for immunostaining), anti-α-tubulin antibodies (used at a dilution of 1:1000 for Western blotting), and protein G-agarose beads were purchased from Santa Cruz Biotechnology (Santa Cruz, CA). Anti-βIII tubulin antibody was purchased from COVANCE (Berkeley, CA) and used at a dilution of 1:1000 for immunostaining. Anti-GFP (used at a dilution of 1:1000 for Western blotting and 1:200 for immunoprecipitation) and anti-GAP43 antibodies were purchased from GeneTex (San Antonio, TX) and used at a dilution of 1:1000 for Western blotting. Anti-actin antibody was purchased from Sigma and used at a dilution of 1:200 for immunostaining. IRDye800CW-labeled anti-rabbit and IRDye680CW-labeled anti-mouse secondary antibodies were purchased from LI-COR Bioscience (Lincoln, NE). Alexa Fluor fluorescence-conjugated secondary antibodies (AF350, AF488, AF555, and AF647), minimum essential media, neurobasal medium, and B-27 serum-free supplement were purchased from Invitrogen. Dulbecco's modified Eagle's medium, horse serum, fetal bovine serum (FBS), L-glutamine (Gln), antibiotic-antimycotic, rhodamine phalloidin, 4′,6-diamidino-2-phenylindole (DAPI), and Lipofectamine 2000 were purchased from Invitrogen. Protease inhibitors, including aprotinin and leupeptin, were purchased from Roche Applied Science. Enhanced chemiluminescence (ECL) reagent was purchased from PerkinElmer Life Sciences. Mammalian transfection system-calcium phosphate reagent was purchased from Promega (Madison, WI).

Plasmids—pEGFP-C1, GFP-SH2B1β(1–670), GFP-SH2B1β-(270–670), GFP-SH2B1β(397–670), GFP-SH2B1β(505–670), GFP-SH2B1β(1–150), GFP-SH2B1β(1–260), and myc-SH2B1β were generous gifts from Dr. Christin Carter-Su at University of Michigan. IRSp53/pCMV-SPORT6 was purchased from Thermo Fisher Scientific (Waltham, MA). Full-length IRSp53(1–521) cDNAs were both subcloned into pRK5-myc via BamHI-EcoRI sites.

Primary Neuronal Culture and 293T Cell Culture—Sprague-Dawley rats were purchased from BioLASCO Taiwan Co., Ltd. Cortical or hippocampal neurons were dissociated from hippocampus dissected from rat embryos (18th day of gestation; E18) by treatment with papain solution (10 units/ml). The isolated primary neurons ($1–2 \times 10^5$/ml) were seeded on a poly-L-lysine (30 ng/ml)-coated dish or coverslip. On day *in vitro* (DIV) 0, primary neurons were cultured in minimum essential media/high glucose medium supplemented with 5% FBS and 5% horse serum under 5% CO_2 conditions. On DIV 1, cells were cultured in neurobasal medium with B27 (containing additional glutamine (Gln) and 0.025 mM glutamate). On DIV 2, cells were treated with 5 μM cytosine-1-β-D-arabinofuranoside to inhibit the growth of glial cells. On DIV 3, cells were cultured in neurobasal and Gln medium (neurobasal medium with B27 containing additional Gln), and then half of the neurobasal and Gln medium was replaced by fresh medium every 3 days. Lipofectamine 2000 or calcium phosphate reagents were used to transfect primary neurons according to the manufacturer's instruction. 1.5–3 h after transfection, culture medium was replaced with fresh medium. 293T cells were grown in DMEM containing 10% FBS, 1% L-Gln, and 1% antibiotic/antimycotic under 5% CO_2 conditions.

Reverse Transcription-Polymerase Chain Reaction (RT-PCR)—TRIzol reagent was used to isolate total RNA from neurons according to the manufacturer's instructions. For reverse transcription, 2 mg of total RNA was converted to cDNA using the reverse transcription kit (Applied Biosystems). SH2B1 isoform primer pairs are as follows: forward 5′-TTCGATATGCTTGAGCACTTCCGG-3′ and reverse 5′-GCCTCTTCTGCCCCAGGATGT-3′. Glyceraldehyde-3-phosphate dehydrogenase (GAPDH) primer pairs are as follows: forward 5′-ACCACAGTCCATGCCATGCCATCAC-3′ and reverse 5′-TCCACCACCCTGTTGCTGTA-3′. The mRNA levels of SH2B1 isoform from RT-PCR were normalized to that of GAPDH.

Knockdown of Endogenous SH2B1—The pLKO.1 lentiviral vector that contains oligonucleotides targeting specific gene sequence pLKO.1-shSH2B1 (clone ID TRCN0000247808 (number 1), 0000247810 (number 2), 0000247809 (number 3), 0000247811 (number 4), 0000247807 (number 5), 0000217475 (number 6), and 0000196146 (number 7)) and pLKO.1-shLacZ (clone ID TRCN0000072236, 0000231717) were purchased from the National Core Facility, located at the Institute of Molecular Biology/Genomic Research Center, Academic Sinica, Taiwan.

Western Blotting, Immunoprecipitation, and Immunofluorescence Staining—Cells were lysed with radioimmunoprecipitation assay buffer, containing 1 mM Na_3VO_4, 1 mM phenylmeth-

ylsulfonyl fluoride (PMSF), 10 ng/ml aprotinin, and 10 ng/ml leupeptin. Equal amounts of proteins were separated by SDS-PAGE and analyzed by Western blotting using the indicated antibodies followed by incubation with IRDye-conjugated secondary antibody. Protein signal was detected using Odyssey infrared imaging system (Odyssey Imager). For immunoprecipitation, cell lysates were incubated with the specific antibody at 4 °C overnight followed by incubation with protein A- or G-agarose beads and rotated at 4 °C for 1 h to pull down specific antibodies. Samples were centrifuged at 2000 rpm at 4 °C for 1 min. The beads were washed three times with radioimmunoprecipitation assay lysis buffer to remove nonspecific binding. The precipitates were dissolved in 1× sample buffer, boiled at 95 °C for 10 min, and analyzed by Western blotting. For immunofluorescence staining, cells were fixed by 4% paraformaldehyde, incubated with the indicated primary antibodies, followed by Alexa Fluor-conjugated secondary antibody. DAPI staining was used to mark the location of the nucleus. Cells were then mounted with Prolong Gold reagent, and the fluorescent images were taken using Carl Zeiss Observer Z1 microscope or Carl Zeiss LSM 510 meta confocal microscope.

GST Pulldown Assay—GST-SH2B1β constructs were expressed in a BL21 strain, and lysates were harvested. GST-SH2B1β proteins were pulled down via glutathione-Sepharose 4B (GE Healthcare). Sepharose beads conjugated with GST-SH2B1β were then incubated with 293T cell lysates for 2 h at 4 °C. Beads were washed and resuspended in SDS sample buffer for Western blotting.

Neurite Outgrowth of PC12 Cells—For nerve growth factor (NGF)-induced neurite outgrowth, PC12-shLacZ or PC12-shSH2B1 cells were split onto collagen I-coated plates at about 20–30% confluency in low serum differentiation medium (DMEM containing 2% horse serum, 1% FBS, 1% antibiotic/antimycotic, and 1% L-Gln). The average length of the longest neurite of cells was determined with ImageJ software. Differentiation of PC12 cells is defined as the length of the neurites being at least twice the diameter of the cell body.

Triton X-100 Cytoskeleton Extraction—Cells were lysed with extraction buffer (0.5% Triton X-100, 100 mM NaF, 50 mM KCl, 2 mM $MgCl_2$, 1 mM EGTA, 10 mM KPO_4, pH 7.5, 0.5 M sucrose) supplemented with protease inhibitors containing 1 mM Na_3VO_4, 1 mM PMSF, 10 ng/ml aprotinin, and 10 ng/ml leupeptin and then centrifuged at 13,000 rpm at 4 °C for 10 min. The supernatant (detergent-soluble fraction containing the G-actin fraction) was taken for immunoblotting. Cell pellets containing F-actin fractions were scraped into the same extraction buffer of the supernatant, and both fractions were solubilized with the same volume of 5× sample buffer. Equal volumes of proteins from each fraction were resolved by SDS-PAGE and detected by Western blotting analysis using the indicated antibodies.

Subcellular Fractionation—Cells were lysed by fractionation buffer (10 mM Tris-HCl, pH 7.9, 10 mM KCl, 0.1 mM EDTA, 0.1 mM EGTA, 1 mM DTT) containing 1 mM Na_3VO_4, 1 mM PMSF, 10 ng/ml aprotinin and leupeptin. Lysates were passed through a 27-gauge needle 50 times and then centrifuged at 2300 rpm (500 × *g*) at 4 °C for 5 min. After centrifugation, the supernatant was removed and transferred to freshly labeled tubes (Thick-wall Polycarbonate) and then centrifuged by an ultracentrifuge

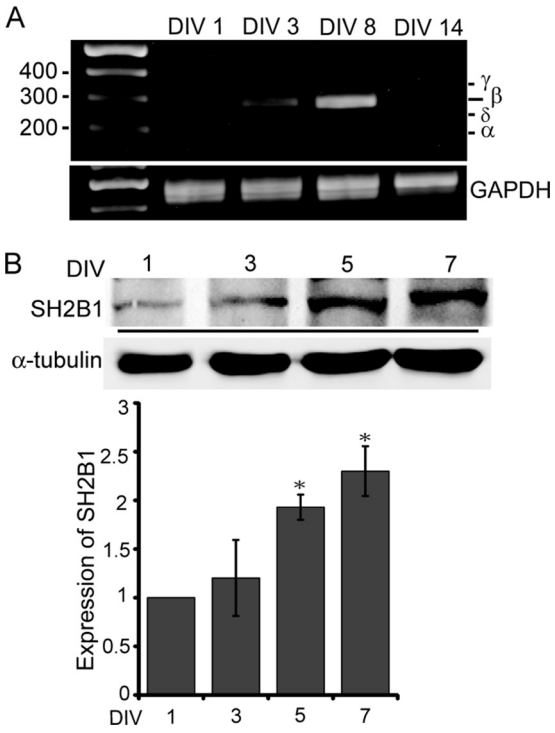

FIGURE 1. **β isoform of SH2B1 is the major isoform during the development of hippocampal neurons.** *A,* RNA was extracted from E18 hippocampal neurons of DIV 1, 3, 8, and 14 and converted to cDNAs for RT-PCR analysis. GAPDH was used as a loading control. *B,* lysates from hippocampal neurons of DIV 1, 3, 5, and 7 were extracted for immunoblotting with anti-SH2B1 or anti-α-tubulin antibody. α-Tubulin was used as a loading control. The relative expression of SH2B1 was quantified by using ImageJ software. *, $p < 0.05$, compared with DIV 1.

(Hitachi, CS150NX, Rotor-S80AT3) at 45,000 rpm (100,000 × *g*) for 1 h. After ultracentrifugation, the supernatant was designated as the cytosolic fraction. The pellet, designated as the membrane fraction, was washed with fractionation buffer and dissolved by lysis buffer. The remaining pellet, designated as the nuclear fraction (nuclei and nucleus-associated structures), was washed twice by fractionation buffer with 0.5% Nonidet P-40 and dissolved by lysis buffer (1% Triton X-100, 1% sodium deoxycholate, 50 mM Tris-HCl, 150 mM NaCl, 1 mM EDTA, 0.1 mM EGTA) containing 1 mM Na_3VO_4, 1 mM PMSF, 10 ng/ml aprotinin and leupeptin.

Measurement of Attachment, End Points, Axon Length, Pearson's Correlation Coefficient, and Co-localization Analysis—The number of attachment and end points was quantified using the built-in cell-counter in ImageJ software (rsb.info.nih.gov, National Institutes of Health, Bethesda). The attachment points are defined as the location where neurite and filopodia connect to the cell body and end point as the location at the tip of filopodia and neurites (28). The average length of the axon was measured using the Simple Neurite Tracer of Fiji software, a plugin in ImageJ software performing semi-automatic tracing of neurons. The mean pixel value of axon length was measured and converted pixels into micrometers (μm). The Pearson's correlation coefficient (*r*) was used to measure the relationship between two variables. Images were analyzed using MetaMorph software (Molecular Devices, Sunnyvale, CA). To examine the correlation between IRSp53 and SH2B1β in hippocampal neurons, cells expressing GFP-SH2B1β were fixed, then

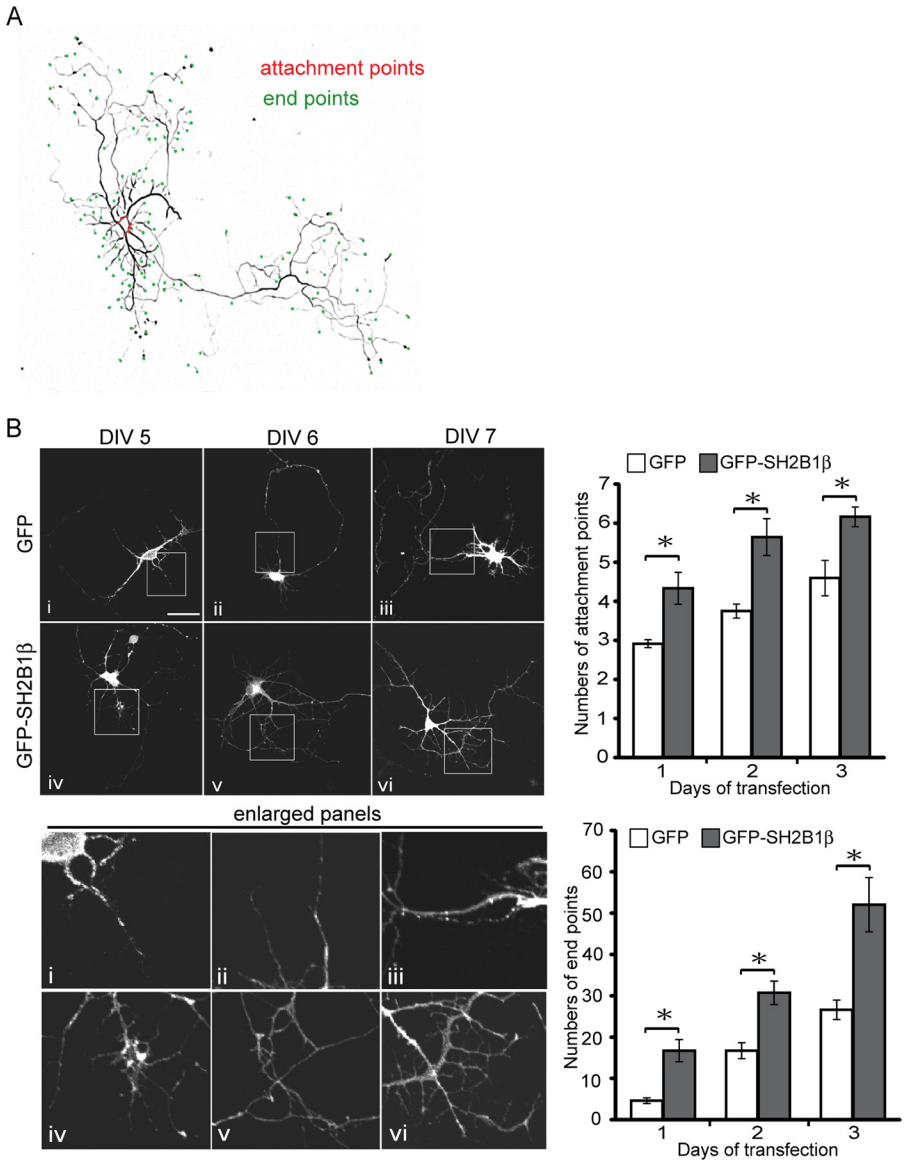

FIGURE 2. **SH2B1β increases branches of neurite in development of hippocampal neurons.** *A,* hippocampal neurons were transiently transfected with GFP-SH2B1β on DIV 3 and images of neuronal morphology were visualized on DIV 7. Attachment points and end points are shown as *red* and *green dots*, respectively. *B,* hippocampal neurons were transiently transfected with either GFP or GFP-SH2B1β on DIV 4, and images of neuronal morphology on days 1–3 after transfection were visualized. Enlarged images of the neurite branches are shown on the *bottom panels. Scale bar,* 40 μm. A total of 12 hippocampal neurons were counted per condition from three independent experiments. Values are mean ± S.E. from three independent experiments and statistically compared by Student's *t* test (*, $p < 0.05$, overexpressing GFP-SH2B1β compared with GFP). The number of attachment points and end points were measured using ImageJ software.

stained with IRSp53, and imaged by using a confocal microscope (Zeiss LSM 510). Both the raw single plane graph of IRSp53 and SH2B1β were quantified by "Co-localization Finder" and "Co-localization Colormap" plugins in ImageJ software. To reach the top 2% overlapping pixels, images should restrain selection to pixels with 85%. Correlation between pair of pixels from IRSp53 and SH2B1β is displayed as distribution of normalized mean deviation product values and visualized with a color scale. Negative indexes are represented by cold colors. Indexes above 0 are represented by hot colors, indicating co-localization. The correlations of IRSp53 and SH2B1β are represented as a color map that is calculated based on Equation 1,

$$\mathrm{nMDP}_{x,y} = \frac{(Ia - \overline{Ia})(Ib - \overline{Ib})}{(Ia_{\max} - \overline{Ia})(Ib_{\max} - \overline{Ib})} \qquad \text{(Eq. 1)}$$

Ia indicates intensity for the given pixel in image a; $\overline{Ia}$ indicates average intensity of image a; $Ia_{\max}$ indicates highest pixel intensity in image a; *Ib* indicates intensity for the given pixel in image b; $\overline{Ib}$ indicates average intensity of image b; and $Ib_{\max}$ indicates highest pixel intensity in image b.

Duolink in Situ Proximity Ligation Assay (PLA)—The Duolink *in situ* PLA assay kit was purchased from Olink Bioscience (Uppsala, Sweden) and was performed according to the manufacturer's instruction. Hippocampal neurons were fixed by 4% paraformaldehyde for 15 min, permeabilized by 0.1% Triton X-100 for 10 min, and incubated with 1% bovine serum albumin in PBS. Neurons were incubated with rabbit anti-SH2B1 antibody and mouse anti-IRSp53 antibodies at 4 °C overnight, followed by incubation with Duolink PLA rabbit PLUS and mouse MINUS probes. After incubation, ligation and

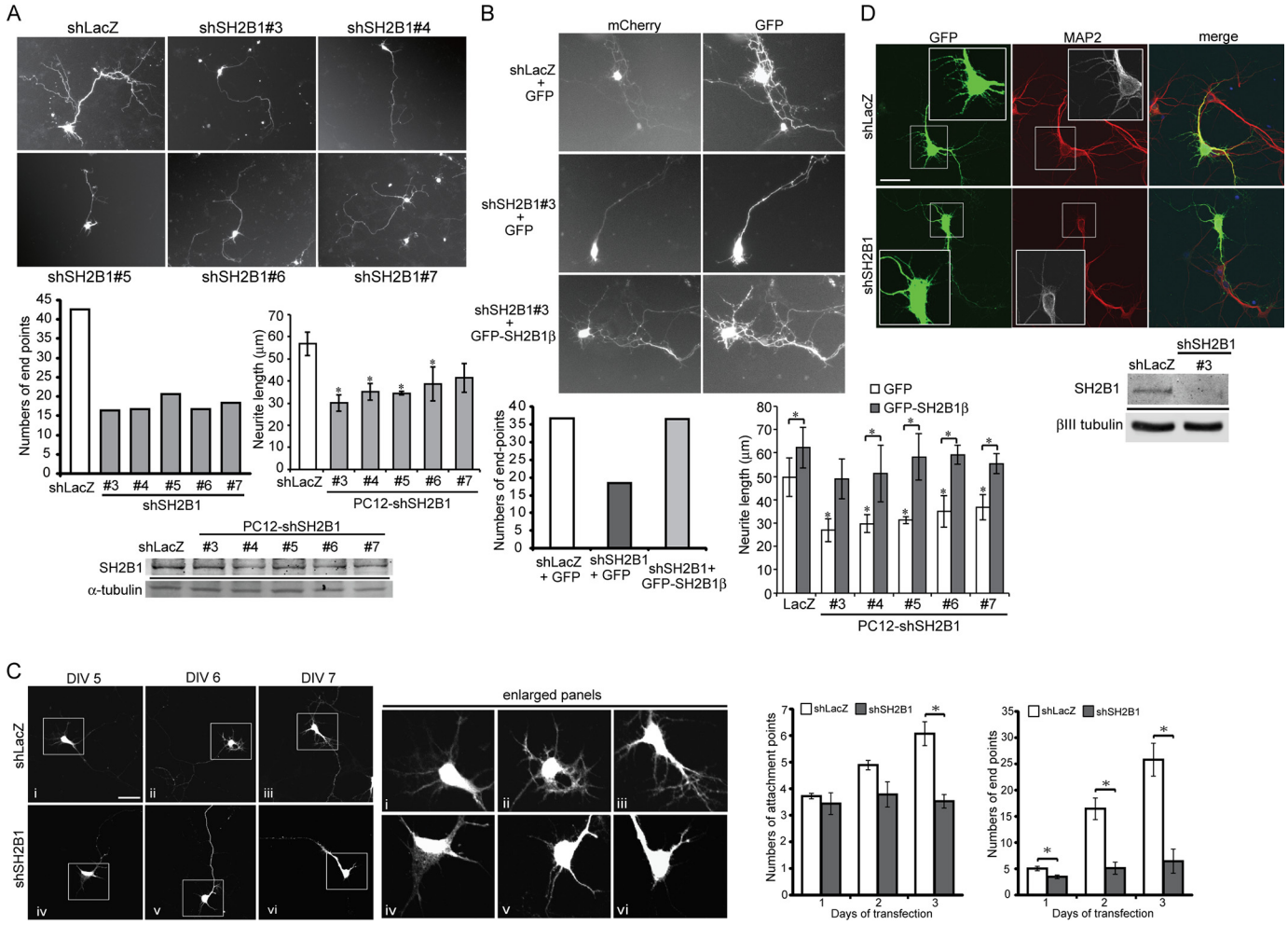

FIGURE 3. **Knockdown of SH2B1 expression reduces neurite outgrowth for hippocampal neurons and PC12 cells.** *A,* hippocampal neurons were transiently transfected with either shLacZ or shSH2B1#3, #4, #5, #6, or #7 together with the pEGFP vector on DIV 4, and live cell images of neuronal morphology were taken. The number of end points was counted from 12 to 18 hippocampal neurons per condition. PC12 cells stably expressing shLacZ or shSH2B1 constructs (shSH2B1#3, #4, #5, #6, and #7) were treated with 100 ng/ml NGF for 1 day. Length of the longest neurite of each cell was calculated from three independent experiments. *, $p < 0.05$ by paired Student's *t* test compared with shLacZ control. Lysates from PC12-shLacZ and PC12-shSH2B1 cells were collected and immunoblotted with anti-SH2B1 and anti-α-tubulin antibodies. *B,* hippocampal neurons were transiently transfected with either shLacZ+mCherry vector or shSH2B1#3+mCherry vector, together with GFP or GFP-SH2B1β on DIV 4, and live cell images were taken. The number of end points was counted from a total of 10–13 hippocampal neurons per condition. PC12-shLacZ or PC12-shSH2B1(*#3, #4, #5, #6,* and *#7*) cells were transiently transfected with GFP or GFP-SH2B1β constructs. Transfected cells were then treated with NGF for 1 day, and the length of the longest neurite of each cell was measured from three independent experiments. *, $p < 0.05$ by paired Student's *t* test compared with PC12-shLacZ+GFP control or with its respective control. *C,* hippocampal neurons were transiently transfected with either shLacZ or shSH2B1 together with pEGFP vector on DIV 4, and images of neuronal morphology on days 1–3 after transfection were taken. The number of attachment points or end points on days 1–3 after transfection was measured. Enlarged images of the neurite branches are shown on the *right panels*. *Scale bar,* 40 μm. A total of 12 hippocampal neurons were counted per condition from three independent experiments. Values are mean ± S.E. from three independent experiments and statistically compared by Student's *t* test (*, $p < 0.05$, shSH2B1 compared with shLacZ). *D,* hippocampal neurons were transfected with either shLacZ or shSH2B1 together with pEGFP vector on DIV 4, and the images of neuronal morphology of were visualized on DIV 7. Immunofluorescence staining was performed with MAP2 (*red*), GFP (*green*), and DAPI (*blue*) antibodies. Cell lysates from cultured hippocampal neurons transiently transfected with shLacZ or shSH2B1(#3) were collected and analyzed via Western blotting with anti-SH2B1 or anti-βIII tubulin antibody.

amplification were followed by using Duolink Detection Reagents Red. Nuclei were stained with DAPI, and cells were mounted using Prolong Gold reagent (Invitrogen). Alexa Fluor 488-phalloidin incubation was used to detect actin structure. Fluorescent signals were obtained by the Carl Zeiss Observer Z1 microscope with a ×100 oil objective.

RESULTS

β Isoform of SH2B1 Is the Major Isoform during in Vitro Culture of Hippocampal Neurons—To study the role of SH2B1 during the development of the central nervous system, we first determined whether the splice variants of SH2B1 are differentially expressed during the development of neurites. Hippocampal neurons were isolated from embryonic day 18 (E18) of rat brain and cultured *in vitro*. RNA levels of the four splice variants of SH2B1 from DIV 1, 3, 8, and 14 hippocampal neurons were compared via RT-PCR. As shown in Fig. 1*A*, mRNA level of β isoform increased on DIV 3, remained high through DIV 8, and decreased by DIV 14. Protein levels of SH2B1 were also up-regulated during early development of hippocampal neurons and a more than 2-fold increase on DIV 7 (Fig. 1*B*). These results indicate that the expression of SH2B1 is increased, and SH2B1β is the predominant isoform during neural differentiation.

SH2B1β Increases Neurite Branches of Hippocampal Neurons—To provide better analysis of the effect of SH2B1 on morphogenesis of hippocampal neurons, E18 hippocampal

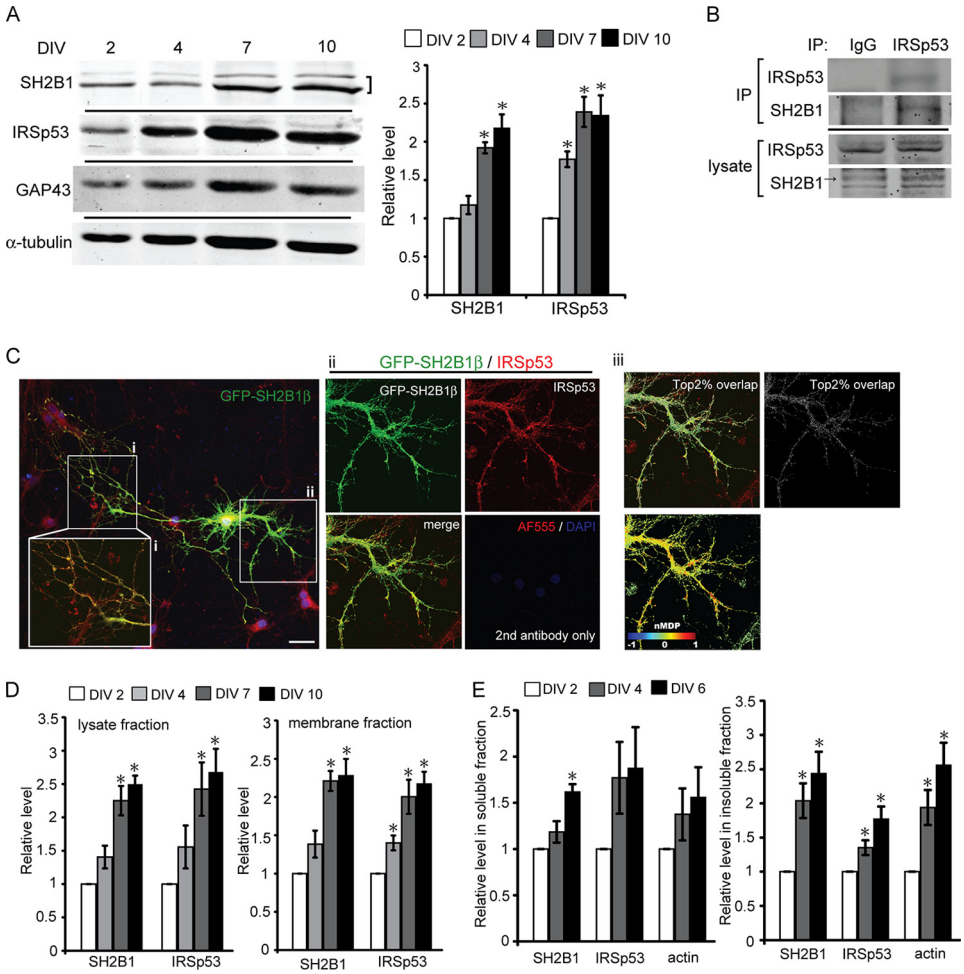

FIGURE 4. **SH2B1β enhances F-actin assembly by interacting with IRSp53 in neuronal differentiation.** *A,* cell lysates from cultured hippocampal neurons on DIV 2, 4, 7, and 10 were collected and analyzed via SDS-PAGE and immunoblotted with anti-SH2B1, IRSp53, GAP-43, and α-tubulin antibodies. SH2B1 and IRSp53 expression levels were normalized to α-tubulin (*, $p < 0.05$, Student's *t* test, compared with DIV 2). *B,* cell lysates from cortical neurons on DIV 10 were collected and subjected to immunoprecipitation (*IP*) using anti-IgG or anti-IRSp53 antibodies followed by immunoblotting with anti-IRSp53 and anti-SH2B1 antibodies. *C,* hippocampal neurons were transiently transfected with GFP-SH2B1β on DIV 4 and subjected to immunofluorescent staining using anti-IRSp53 (*red*) antibody together with DAPI (*blue*). *Scale bar,* 40 μm. Enlarged images of the neurite branches (*panels i* and *ii*) are shown on the *bottom* and *right panels*. *Panel iii,* top 2% of overlapped pixels of GFP-SH2B1β and IRSp53 on the neurite branches (*panel ii*) was superimposed on IRSp53 images as displayed in *white*. Correlation between paired pixels of IRSp53 and SH2B1β was also displayed as normalized mean deviation product color map. Indexes above 0 are represented in *red*, indicating co-localization. *Scale bar,* 40 μm. *D,* whole cell lysates and membrane fractionation levels of SH2B1 and IRSp53 on DIV 2, 4, 7, and 10 were quantified (*, $p < 0.05$, Student's *t* test, compared with DIV 2). *E,* cell lysates from hippocampal neurons of DIV 2, 4, and 6 were collected. Triton X-100 detergent of soluble G-actin and insoluble F-actin fractions was equally subjected to immunoblotting with anti-SH2B1, IRSp53, and actin. The relative expression levels were quantified on DIV 2, 4, and 6 in soluble and insoluble fractions (*, $p < 0.05$, Student's *t* test, compared with DIV 2).

neurons were transiently transfected with GFP or GFP-SH2B1β on DIV 4, and morphology of neurons was imaged on DIV 5–7. Quantification of the attachment points and end points, symbolic of neurites and neurite branches, respectively (28), is shown in Fig. 2*A*. Overexpression of SH2B1β increased the numbers of attachment points and end points (Fig. 2*B*). If SH2B1 is required for neurite outgrowth, knocking down SH2B1 would reduce neurite outgrowth. Five shSH2B1 constructs were tested for the efficiency of knocking down SH2B1. Hippocampal neurons were transfected with GFP together with either shLacZ or shSH2B1(numbers 3–7). Endogenous SH2B1 was differentially reduced by these shSH2B1, and the numbers of end points were reduced. The effect of shSH2B1 on neurite length of PC12 cells were also reduced (Fig. 3*A*). The relative reduction of endogenous SH2B1 protein by each shSH2B1 construct is shown (Fig. 3*A*, *bottom panel*). In the following experiments, we used shSH2B1#3 for morphogenesis analysis. To verify that the reduced end points and neurite length resulted specifically from knockdown of SH2B1, rescue experiments were performed. Hippocampal neurons were transiently transfected with shLacZ or shSH2B1 plus mCherry vector to mark the transfected neurons, together with GFP or GFP-SH2B1β overexpression to examine the rescue effect. End points were counted and compared. As shown in Fig. 3*B*, shSH2B1 reduced the number of end points, and expressing GFP-SH2B1β rescued the neurite branching back to the level of shLacZ control. Similar experiments were performed using PC12 cells and putting back SH2B1β also rescued the reduced neurite length by shSH2B1 (Fig. 3*B*). By comparing the attachment and end points, knockdown of SH2B1 significantly reduced the number of end points most dramatically, with 75% reduction 3 days after transfection compared with shLacZ control (Fig. 3*C*). Moreover, knocking down shSH2B1 led to the reduced numbers of primary dendrites as

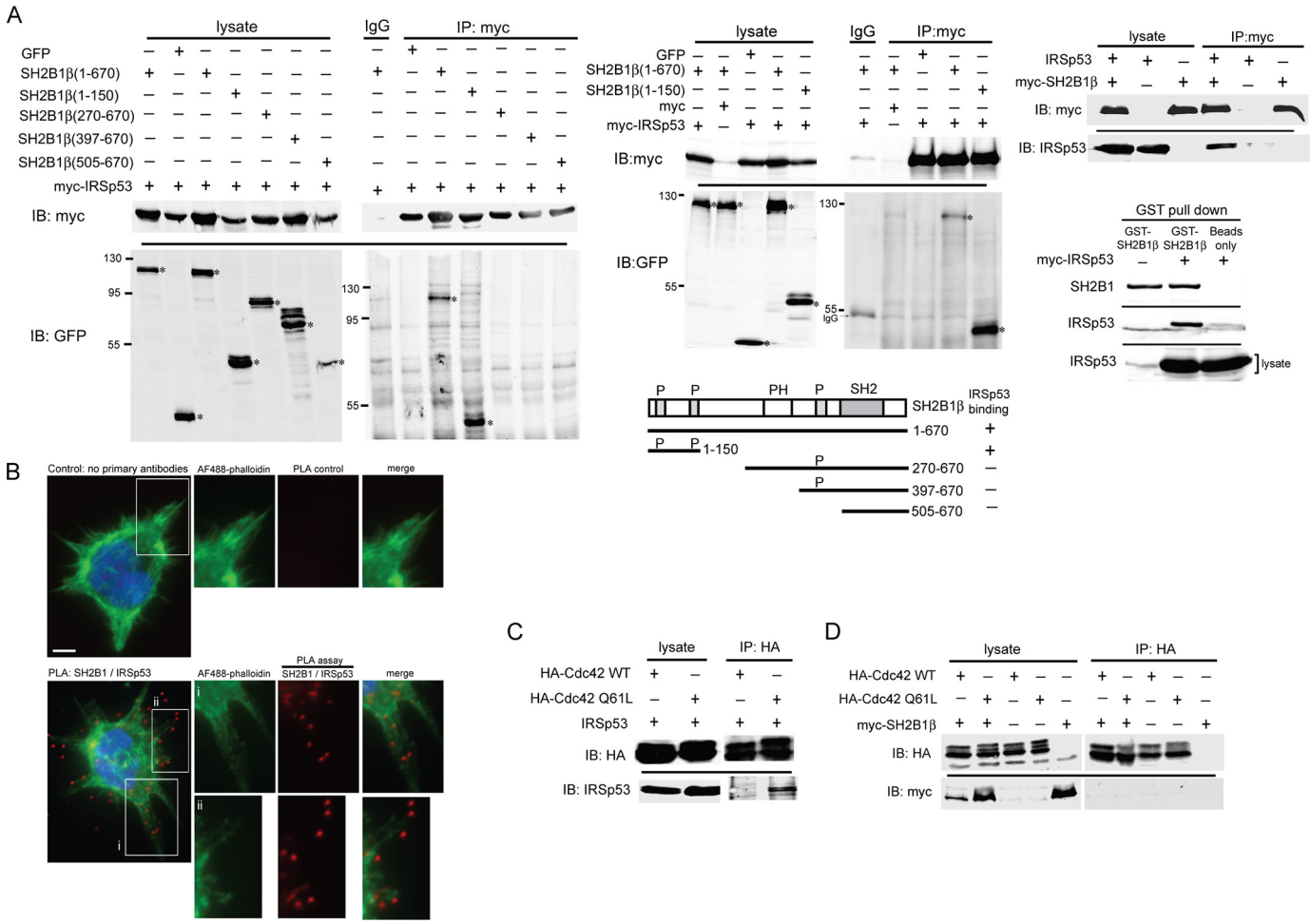

FIGURE 5. **Proline-rich domains of SH2B1β interact with IRSp53.** *A,* GFP, GFP-SH2B1β(1–670), or truncated SH2B1β and Myc vector or myc-IRSp53 constructs were transiently co-transfected to 293T cells. Cell lysates were collected and subjected to immunoprecipitation (*IP*) with anti-Myc antibody and immunoblotted (*IB*) with anti-Myc and GFP antibodies. In the reverse co-immunoprecipitation experiment, myc-SH2B1β with or without IRSp53 was transfected to 293T cells. Cell lysates were collected and subjected to immunoprecipitation with anti-Myc antibody and immunoblotted with anti-Myc or anti-IRSp53 antibody. GST-SH2B1β was purified via glutathione-Sepharose beads. Cell lysates from 293T cells transiently transfected with Myc or myc-IRSp53 were incubated with Sepharose beads only or beads conjugated with GST-SH2B1β. Pulldown of the GST-SH2B1β-containing complex was subjected to Western blotting with anti-SH2B1 and anti-IRSp53 antibodies. * indicates the specific bands. *B,* hippocampal neurons were fixed, permeabilized, and incubated with anti-SH2B1 and anti-IRSp53 antibodies followed by reaction with Duolink PLA probes and reagents. Neurons incubated with Duolink PLA probes served as the negative control. Images were taken using Carl Zeiss Observer Z1 microscope. F-actin and nucleus were visualized by staining with Alexa Fluor 488-phalloidin and DAPI, respectively. *Scale bar,* 10 μm. *C,* 293T cells were transiently transfected with IRSp53 and HA-Cdc42WT (wild-type Cdc42) or HA-Cdc42(Q61L) (constitutively active form of Cdc42). Lysates were collected and subjected to immunoprecipitation using anti-HA antibody followed by immunoblotting with anti-IRSp53 and anti-HA antibodies. *D,* 293T cells were transiently transfected with myc-SH2B1β and HA-Cdc42WT or HA-Cdc42(Q61L). Lysates were collected and immunoprecipitated with anti-HA antibody followed by immunoblotting with anti-HA and Myc antibodies.

demonstrated by the staining of the dendritic marker, microtubule-associated protein 2 (MAP2) (Fig. 3*D*). These findings suggest that SH2B1 is required for the growth of dendrites and their branches.

SH2B1 Interacts with IRSp53—The formation of actin-rich filopodia precedes the formation of neurites (1). To determine whether SH2B1 may promote dendrite formation by enhancing filopodium formation, we set out to examine the expression of a known filopodium-regulating protein, IRSp53. For hippocampal neurons cultured *in vitro*, the expressions of endogenous IRSp53 increased. Similarly, the expressions of SH2B1 and the differentiation marker growth-associated protein 43 (GAP43) were increased over time (Fig. 4*A*). IRSp53 is an IMD domain-containing protein known to promote membrane protrusion. To examine whether SH2B1 is in the IRSp53-containing complexes, endogenous IRSp53 was immunoprecipitated from the lysate of cortical neurons, and the presence of endogenous SH2B1 was examined. As demonstrated in Fig. 4*B*, SH2B1 existed in the IRSp53-containing complexes.

Whether SH2B1 actively participates in the IRSp53-dependent membrane protrusion, they should co-localize at the plasma membrane fraction. Hippocampal neurons were transiently transfected with GFP-SH2B1β, and immunofluorescence staining of IRSp53 was performed to visualize the potential co-localization of SH2B1 and IRSp53. As revealed in Fig. 4*C*, GFP-SH2B1β and IRSp53 co-localize mostly at the branch points as well as the tips of neurites. The co-localization between SH2B1 and IRSp53 was also analyzed by Pearson's correlation coefficient (= 0.8) and showed a high level of co-localization. The top 2% overlapped pixels of GFP-SH2B1β and IRSp53 on the neurite branches are shown in white (Fig. 4*C*, *panel iii*). To complement the single cell assays, fractionation

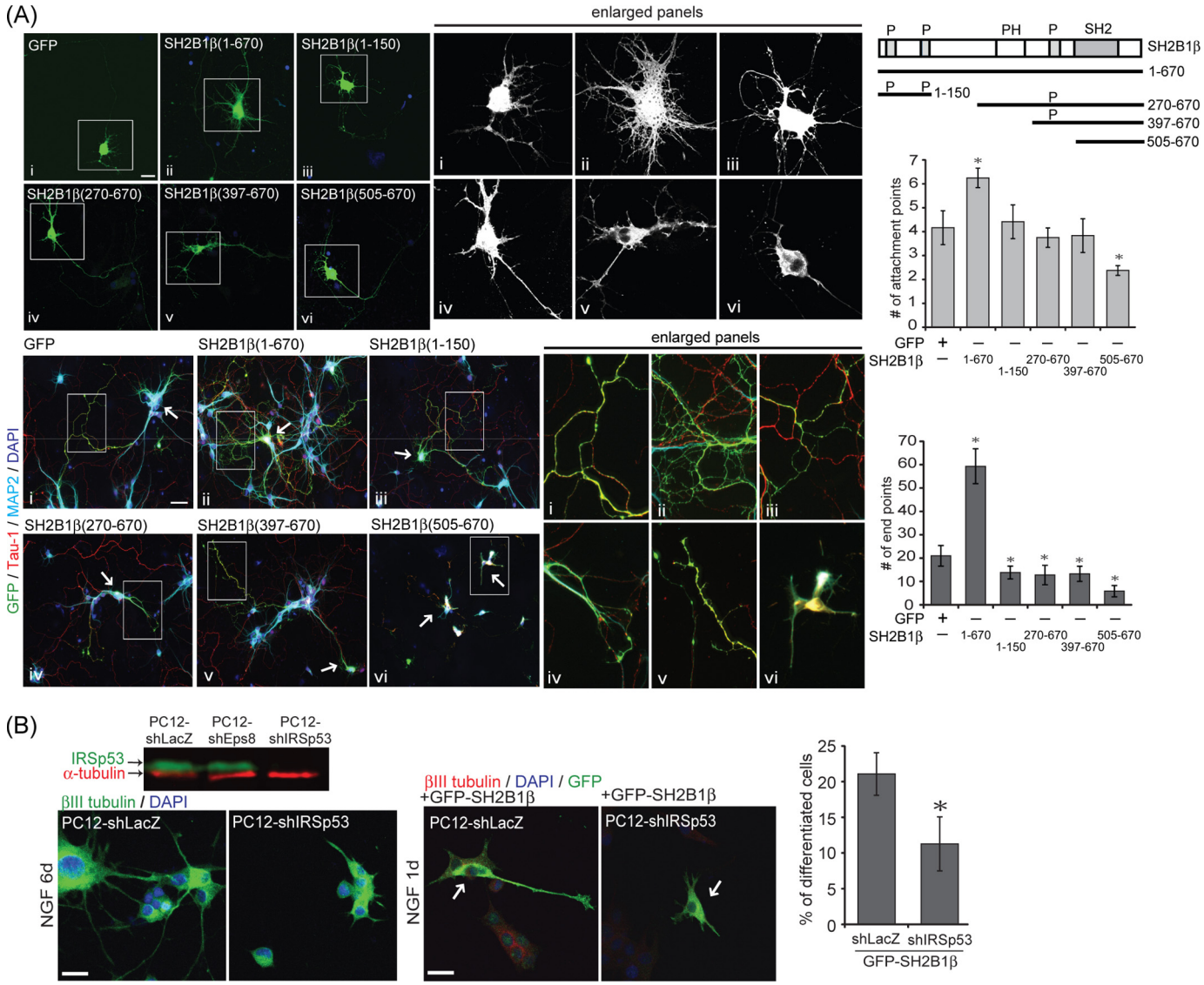

FIGURE 6. **Proline-rich domains of SH2B1β are required to enhance filopodium formation and neurite outgrowth in hippocampal neurons.** *A,* schematics of full-length (1–670) and various truncated SH2B1β structures. Amino acid numbers are shown. *Top two panels,* GFP (*panel i*), full-length (*panel ii*), or truncated form (*panels iii–vi*) of SH2B1β constructs were transiently transfected to hippocampal neurons on DIV 3, and images of the live neurons were taken on DIV 7 using Zeiss Observer Z1 microscope. Enlarged images of the neurite branches and filopodium formation are shown on the *right panels*. *Scale bar,* 20 μm. A total of 15 cells were counted per condition from three independent experiments. Values are mean ± S.E. from three independent experiments (*, $p <$ 0.05, Student's *t* test, overexpressing full-length and truncated form of SH2B1β constructs compared with GFP). *Bottom two panels*, GFP (*panel i*), full-length (*panel ii*), or truncated form (*panels iii–vi*) of SH2B1β constructs were transiently transfected to hippocampal neurons on DIV 4, and the morphology of the neurons was subjected to immunofluorescence staining with anti-MAP2 (*light blue*) and Tau-1 (*red*) antibodies together with DAPI (*blue*) on DIV 7. The *arrows* show the overexpression of GFP, full-length, or truncated form of SH2B1β in hippocampal neurons. *Scale bar,* 40 μm. *B,* PC12 cells stably expressing shLacZ (*PC12-shLacZ*) or shIRSp53 (*PC12-shIRSp53*) were established. Cell lysates from PC12-shLacZ, PC12-shEps8, and PC12-shIRSp53 cells were collected and immunoblotted with anti-IRSp53 and α-tubulin antibodies. *Left two panels,* PC12-shLacZ and PC12-shIRSp53 cells treated with 50 ng/ml NGF for 6 days were subjected to immunofluorescent staining with anti-βIII tubulin (*green*) antibody together with DAPI (*blue*). *Scale bar,* 20 μm. *Right two panels,* PC12-shLacZ and PC12-shIRSp53 cells were transiently transfected with GFP-SH2B1β and then treated with 50 ng/ml NGF for 1 day before immunofluorescent staining with anti-βIII tubulin (*red*) and GFP (*green*) antibodies together with DAPI (*blue*). The *arrows* show overexpression of GFP-SH2B1β in PC12-shLacZ and PC12-shIRSp53 cells. *Scale bar,* 20 μm. A total 100–105 cells were counted per condition from three independent experiments. Values are mean ± S.E. from three independent experiments (*, $p <$ 0.05, Student's *t* test, PC12-shIRSp53 compared with PC12-shLacZ).

experiments were performed to examine the subcellular distribution of endogenous SH2B1 and IRSp53 in the plasma membrane fraction. As the expression of the endogenous SH2B1 and IRSp53 increased during the formation of the neurite network of hippocampal neurons (Fig. 4*A*), SH2B1 and IRSp53 increased 2-fold at the plasma membrane fraction on DIV 7 and DIV 10 (Fig. 4*D*, *right panel*). The initiation and formation of the prospective neurites require the assembly of G-actin to F-actin. To delineate whether SH2B1-IRSp53 complexes may reside with polymerized F-actin, cell lysates of hippocampal neurons from DIV 2 to 6 were collected for fractionation to separate detergent-soluble and -insoluble fractions. The endogenous SH2B1 and IRSp53 were obviously in the detergent-insoluble fraction containing polymerized F-actin on DIV 4 and DIV 6 compared with DIV 2 (Fig. 4*E*).

The fact that SH2B1β and IRSp53 interact and co-localize, we next examined which region(s) of SH2B1β is required for their interaction. To this end, SH2B1 or various truncation

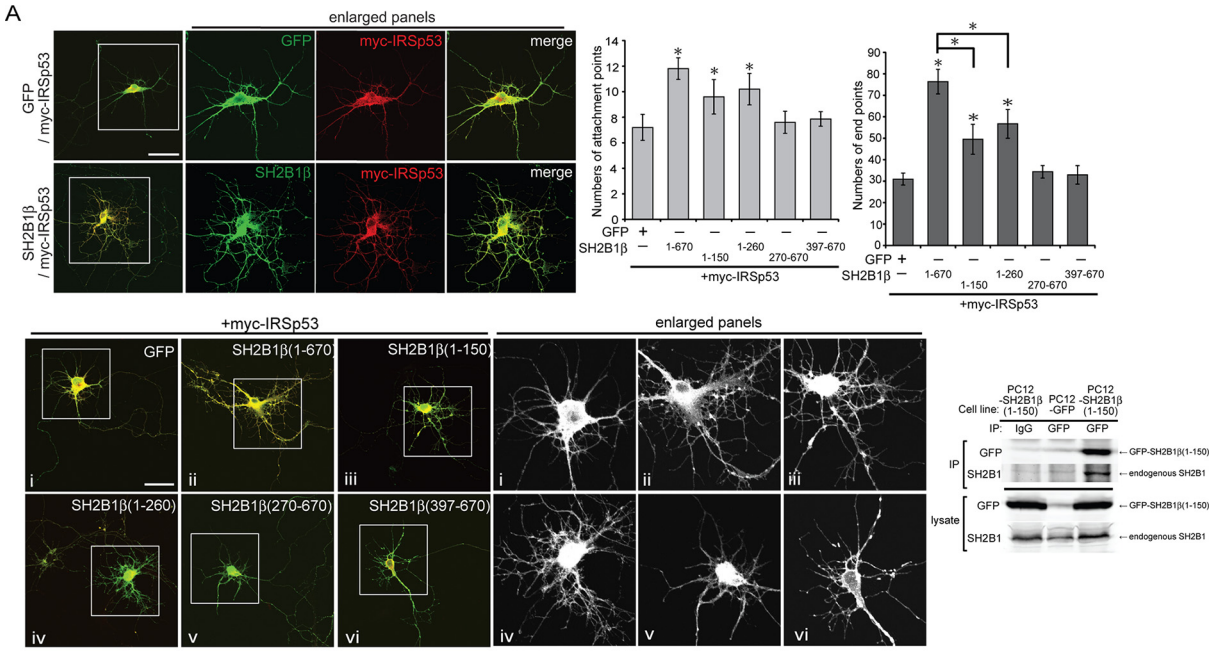
A
enlarged panels
GFP
myc-IRSp53
merge
GFP / myc-IRSp53
SH2B1β
SH2B1β / myc-IRSp53
Numbers of attachment points
Numbers of end points
GFP
SH2B1β
1-670
1-150
1-260
270-670
397-670
+myc-IRSp53
+myc-IRSp53
enlarged panels
SH2B1β(1-670)
SH2B1β(1-150)
SH2B1β(1-260)
SH2B1β(270-670)
SH2B1β(397-670)
PC12 -SH2B1β (1-150)
PC12 -GFP
Cell line:
IP:
IgG
IP
lysate
GFP-SH2B1β(1-150)
endogenous SH2B1

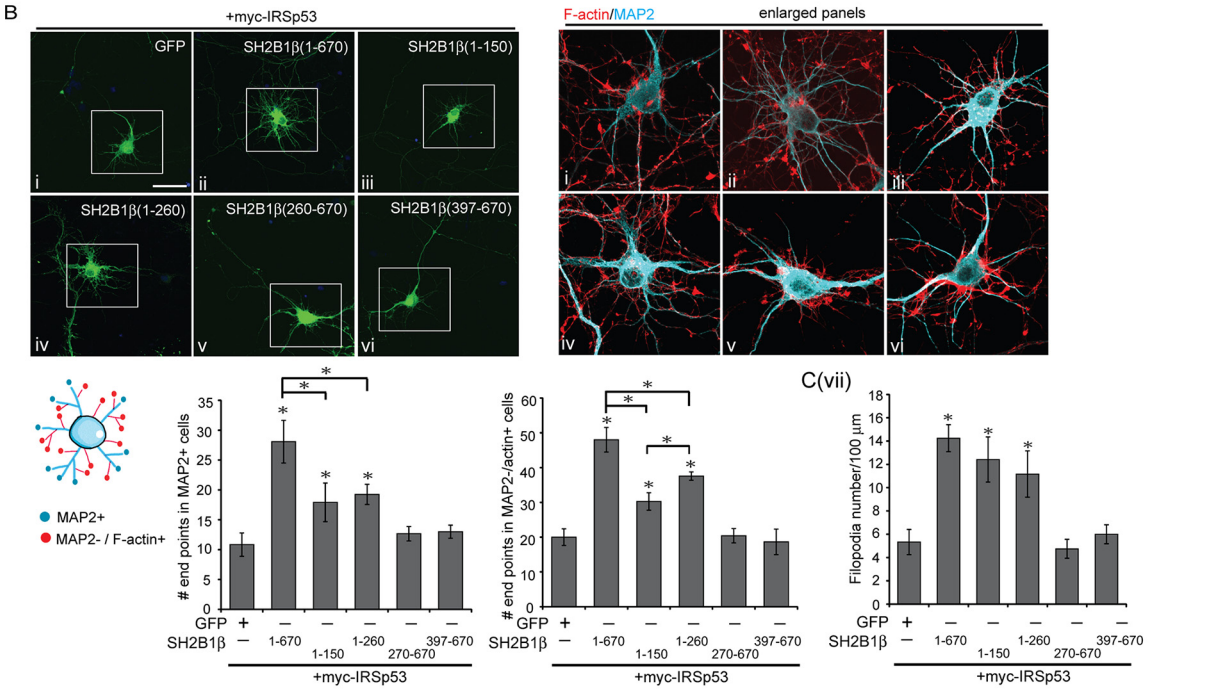
B
+myc-IRSp53
F-actin/MAP2
enlarged panels
GFP
SH2B1β(1-670)
SH2B1β(1-150)
SH2B1β(1-260)
SH2B1β(260-670)
SH2B1β(397-670)
MAP2+
MAP2- / F-actin+
# end points in MAP2+ cells
# end points in MAP2-/actin+ cells
C(vii)
Filopodia number/100 µm
GFP
SH2B1β
1-670
1-150
1-260
270-670
397-670
+myc-IRSp53

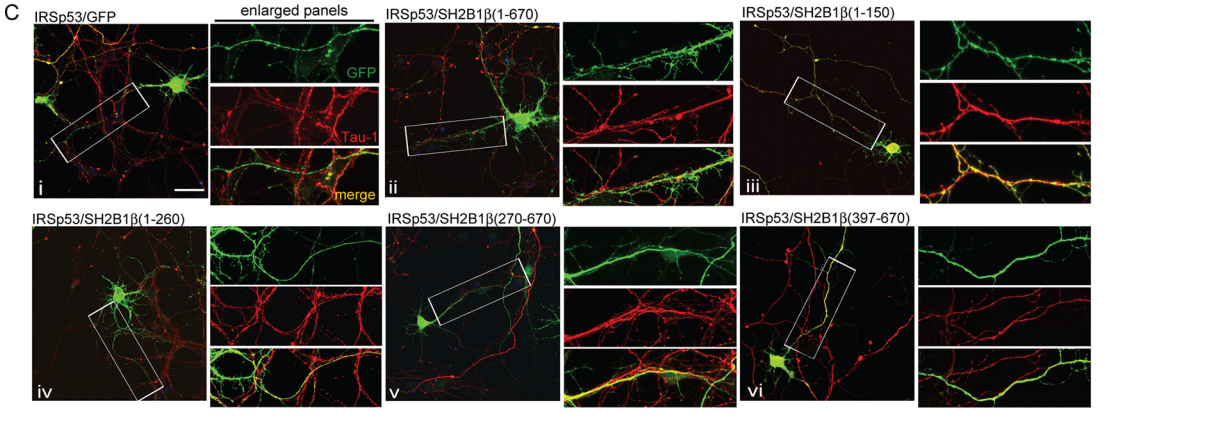
C
IRSp53/GFP
enlarged panels
GFP
Tau-1
merge
IRSp53/SH2B1β(1-670)
IRSp53/SH2B1β(1-150)
IRSp53/SH2B1β(1-260)
IRSp53/SH2B1β(270-670)
IRSp53/SH2B1β(397-670)

mutants of SH2B1β, including SH2B1β(1–150), SH2B1β(270–670), SH2B1β(397–670), and SH2B1β(505–670), were used to transfect 293T cells together with myc-IRSp53. IRSp53 was immunoprecipitated, and the presence of SH2B1β or its mutants was examined. As in Fig. 5*A*, SH2B1β and SH2B1β(1–150) interacted with IRSp53. SH2B1β(270–670), SH2B1β-(397–670), and SH2B1β(505–670) did not. This result suggests that SH2B1β likely interacts with IRSp53 through its N-terminal proline-rich domains. Reverse co-immunoprecipitation was also performed through immunoprecipitating myc-SH2B1β and re-probed with anti-IRSp53. *In vitro* GST-SH2B1β pull-down assay also detected IRSp53 in the same complex (Fig. 5*A, right panels*). To confirm the *in vitro* interaction results, Duolink *in situ* PLA assays were used to examine the *in vivo* association between endogenous SH2B1β and IRSp53 in hippocampal neurons. Hippocampal neurons were incubated with anti-SH2B1 and anti-IRSp53 antibodies followed by reaction with *in situ* PLA assay probes and reagents. The interaction between SH2B1 and IRSp53 was detected by red fluorescent puncta. In addition, actin structure was visualized by Alexa Fluor 488-phalloidin staining. As shown Fig. 5*B*, the SH2B1-IRSp53 complexes existed at the plasma membrane, actin, and filopodium tips. During the elongation of actin filaments, IRSp53 recruits VASP to the site of action, and this recruitment is regulated by Cdc42 (29, 30). To examine whether IRSp53 interacts with Cdc42, 293T cells were transfected with IRSp53 together with HA-Cdc42 or the constitutive active form of Cdc42, HA-Cdc42(Q61L). When immunoprecipitating with anti-HA antibody, IRSp53 was in the same complex with HA-Cdc42(Q61L) (Fig. 5*C*). This result raised the possibility that SH2B1 may interact with Cdc42 or VASP instead of directly with IRSp53. Nonetheless, SH2B1β does not interact with VASP (31). Thus, we examined the possible interaction of SH2B1β and Cdc42. As shown in Fig. 5*D*, SH2B1β did not interact with either wild-type Cdc42 or the constitutive active form, Cdc42(Q61L).

Proline-rich Domains of SH2B1β Are Required to Enhance Filopodium Formation and Neurite Outgrowth in Hippocampal Neurons—To determine which region(s) of SH2B1β is required for enhancing filopodium formation and neurite outgrowth, various truncation mutants of GFP-SH2B1β were transfected to hippocampal neurons, and the numbers of attachment points and end points were quantified. As shown in Fig. 6*A*, overexpressing full-length GFP-SH2B1β significantly enhanced the numbers of attachment points and end points in hippocampal neurons compared with control GFP cells. SH2B1β truncation mutants cannot increase the attachment points. In contrast, overexpressing these mutants significantly reduced the number of end points of hippocampal neurons compared with GFP-expressing cells. It is possible that SH2B1β(1–150) titrates out the limiting amount of endogenous IRSp53, whereas SH2B1β(270–670) and SH2B1β(397–670) may bind to and sequester other filopodia regulating proteins. Overexpression of SH2B1β(505–670), lacking all three N- and C-terminal proline-rich domains, inhibited both attachment and end points. This finding could result from the SH2 domain only mutant, SH2B1β(505–670), sequestering the neurotrophin receptors required for neurite outgrowth. Neuronal markers of dendrites and axons were also determined. Fixed neurons were subjected to immunofluorescence staining with anti-MAP2 (dendritic marker), Tau-1 (axonal marker), and DAPI. Overexpressing truncated mutants of SH2B1β significantly reduced the dendritic or axonal filopodia and neurite branching compared with overexpressing full-length GFP-SH2B1β cells. Interestingly, overexpressing GFP-SH2B1β lacking both N- and C-terminal proline-rich domains strongly blocked the filopodium formation and neurite outgrowth. These results suggest that the N- and C-terminal proline-rich domains of SH2B1β are required for enhancing the formation of filopodia and neurite branching during neural development. To determine whether SH2B1β-mediated neurite outgrowth depends on IRSp53, the stable cell line PC12-shLacZ and PC12-shIRSp53 were established. As shown in the immunoblot, the protein level of IRSp53 was significantly reduced (Fig. 6*B*). Neurite outgrowth was inhibited in PC12-shIRSp53 cells and cannot be rescued by putting back GFP-SH2B1β. These results suggest that IRSp53 is required for SH2B1β-enhanced filopodium formation and neurite outgrowth.

N-terminal Proline-rich Domains of SH2B1β Enhance IRSp53-induced Neurite Outgrowth—To examine whether interaction between SH2B1 and IRSp53 is required to enhance IRSp53-induced neurite outgrowth, hippocampal neurons were transiently transfected with myc-IRSp53 together with GFP, GFP-SH2B1β, GFP-SH2B1β(1–150), GFP-SH2B1β(1–260), GFP-SH2B1β(270–670), or GFP-SH2B1β(397–670). The morphology of neurons was examined, and the numbers of attachment points as well as end points were quantified. The co-expression of SH2B1 and IRSp53 is shown in Fig. 7*A*. Overexpressing SH2B1β and IRSp53 increased both attachment (1.7-fold) and end (2.5-fold) points, whereas overexpression of

FIGURE 7. **SH2B1β and IRSp53 synergistically regulate the formation of dendritic and axonal filopodia during neurite outgrowth.** *A,* GFP (*panel i*), full-length (*panel ii*) or truncated form (*panels iii–vi*) of SH2B1β constructs were transiently co-transfected with myc-IRSp53 to hippocampal neurons on DIV 4, and the images of neuronal morphology were taken on DIV 7. Neurons were subjected to immunofluorescent staining with anti-Myc (*red*) and GFP (*green*). Enlarged images of the neurite branches and filopodium formation for GFP channel are shown in the *right panels*. *Scale bar,* 40 μm. A total of 15 cells were counted per condition from three independent experiments. Values are mean ± S.E. from three independent experiments (*, $p < 0.05$, Student's *t* test). PC12 cells stably expressing GFP or GFP-SH2B1β(1–150) were immunoprecipitated using anti-IgG or anti-GFP antibodies. Immunoprecipitated complexes were resolved and immunoblotted using antibodies against anti-GFP and anti-SH2B1 antibodies. *B,* GFP (*panel i*), full-length (*panel ii*), or the truncated form (*panels iii–vi*) of SH2B1β constructs were transiently co-transfected with myc-IRSp53 to hippocampal neurons on DIV 4, and the morphology of the neurons was visualized on DIV 7. Enlarged images of the dendritic filopodia and branches are shown in the *right panels*. Neurons were subjected to immunofluorescence staining with anti-MAP2 (Cy5) and GFP (*green*) antibodies and F-actin (*red*). The end points of MAP2+ or MAP2-/F-actin+ signal were quantified to analyze the filopodial and dendritic branches. MAP2 was highlighted in *light blue* for observation. *C,* GFP (*panel i*), full-length (*panel ii*), or truncated from (panels iii–vi) of SH2B1β constructs were transiently co-transfected with myc-IRSp53 to hippocampal neurons on DIV 4, and the morphology of the neurons was visualized on DIV 7. Enlarged images of the axonal filopodia are shown in the *right panels*. Neurons were subjected with immunofluorescence staining with anti-GFP (*green*) and Tau-1 (*red*) antibodies together with DAPI (*blue*). *Scale bar,* = 40 μm. *Panel vii,* axonal filopodia were quantified per 100 μm. Total 12 cells were counted per condition from three independent experiments. Values are mean ± S.E. from three independent experiments (*, $p < 0.05$, Student's *t* test).

IRSp53 together with SH2B1β(1–150) or SH2B1β(1–260) increased attachment points 1.4-fold and end points ~2-fold compared with IRSp53 and GFP-expressing neurons. Overexpression of IRSp53 and SH2B1β(270–670) or SH2B1β(397–670), however, did not enhance attachment or end points (Fig. 7*A*). The fact that overexpressing SH2B1β(1–150) or SH2B1β(1–260) together with IRSp53 did not exhibit dominant negative or loss-of-function phenotype was likely due to the interaction of SH2B1β(1–150) and endogenous SH2B1 (Fig. 7*A*, *bottom right panel*). Both SH2B1β(1–150) and SH2B1β(1–260) contain the dimerization domain and can bring together full-length SH2B1 to stimulate IRSp53-induced filopodium formation and neurite outgrowth.

To investigate whether the increased dendritic branches by SH2B1β and IRSp53 result from increased actin-rich filopodia, we quantified the relative actin-positive and MAP2-negative end points, representative of filopodia/immature dendrites. Similar to the results from Fig. 7*A*, the relative numbers of filopodia and dendritic branches were increased in neurons overexpressing IRSp53 together with SH2B1β, SH2B1β(1–150), or SH2B1β(1–260). Overexpression of IRSp53 together with SH2B1β(270–670) or SH2B1β(397–670) did not increase dendritic branches compared with control neurons (Fig. 7*B*). By staining with Tau-1, the numbers of filopodia along the axon also increased in neurons overexpressing IRSp53 plus SH2B1β, SH2B1β(1–150), or SH2B1β(1–260) but not in neurons overexpressing IRSp53 plus SH2B1β(270–670) or SH2B1β(397–670) (Fig. 7*C*). These results point to the importance of the N-terminal proline-rich domains of SH2B1β in promoting IRSp53-dependent filopodium formation and neurite outgrowth.

DISCUSSION

Filopodia are generally known to sense environmental cues and to regulate tissue morphogenesis and regeneration. However, exactly how filopodia are initiated at a specific locale remains unclear. IRSp53 has been well documented in promoting membrane protrusion and filopodium formation. In this study, we demonstrate that SH2B1 interacts with IRSp53 and promotes neurite outgrowth and neuronal branching. Based on the known interaction between SH2B1 and neurotrophin receptors at the cell surface during neuronal differentiation (18, 19, 23–25), these results raise the possibility that SH2B1-IRSp53 complexes specify locations for filopodium formation through SH2B1-mediated signaling events. In line with this possibility, overexpression of SH2 domain only mutant, SH2B1β(505–670), inhibits neurite outgrowth (Fig. 6*A*) potentially through sequestering neurotrophin receptors.

The process from membrane protrusion (actin-free) to the formation filopodia (actin-rich) is very dynamic (32). Stabilizing the structure of filopodia is essential for neurite initiation. The fact that overexpression of SH2B1β and IRSp53 promotes the formation of actin-positive (filopodia) and MAP2-negative (immature dendrites) end points suggests that SH2B1β may be recruited or targeted to the plasma membrane to participate in IRSp53-induced membrane protrusion process. Amino acids 150–260 of SH2B1β contain membrane targeting and actin-binding regions (33, 34). Nonetheless, SH2B1β(1–150) and SH2B1β(1–260) showed a similar effect on dendritic and axonal branches (Fig. 7, *B* and *C*). Thus, it is likely that SH2B1 is recruited to the plasma membrane by mechanisms other than using its own membrane targeting region. We show in this study that SH2B1β(1–150), containing two proline-rich regions as well as the dimerization domain, brings together the endogenous SH2B1 to action (Fig. 7*A*).

During actin elongation, IRSp53 is known to recruit VASP to the site of action, and this recruitment is regulated by Cdc42 (29, 30). Nonetheless, SH2B1β does not interact with either VASP (31) or Cdc42 (Fig. 5*D*). An IRSp53-interacting protein is Eps8 (epidermal growth factor receptor kinase substrate 8). Eps8 can cap barbed ends of actin filaments when binding to Abi-1, whereas the association of Eps8 with IRSp53 induces filopodium formation by cross-linking actin filaments (30, 35, 36). These findings suggest that Eps8 can induce or inhibit the filopodium formation depending on its binding proteins. Although published reports suggest the involvement of Eps8 mainly in spine formation, it would be of interest to investigate whether Eps8 is in the complex of SH2B1-IRSp53 to promote filopodium formation and thus spine formation.

Acknowledgments—We thank Dr. Eric Huang from the National Chiao Tung University in Taiwan and Dr. H. Benjamin Peng from Hong Kong University of Science and Technology for the insightful discussion concerning this project. We are also grateful for the technical advice on neural culture from Dr. Yu-Chia Jenny Chou at the National Yang-Ming University and Dr. Yen-Chung Chang at the National Tsing Hua University, Taiwan.

REFERENCES

1. Dent, E. W., Kwiatkowski, A. V., Mebane, L. M., Philippar, U., Barzik, M., Rubinson, D. A., Gupton, S., Van Veen, J. E., Furman, C., Zhang, J., Alberts, A. S., Mori, S., and Gertler, F. B. (2007) Filopodia are required for cortical neurite initiation. *Nat. Cell Biol.* **9,** 1347–1359
2. Kwiatkowski, A. V., Rubinson, D. A., Dent, E. W., Edward van Veen, J., Leslie, J. D., Zhang, J., Mebane, L. M., Philippar, U., Pinheiro, E. M., Burds, A. A., Bronson, R. T., Mori, S., Fässler, R., and Gertler, F. B. (2007) Ena/VASP is required for neuritogenesis in the developing cortex. *Neuron* **56,** 441–455
3. Ahmed, S., Goh, W. I., and Bu, W. (2010) I-BAR domains, IRSp53, and filopodium formation. *Semin. Cell Dev. Biol.* **21,** 350–356
4. Schirenbeck, A., Arasada, R., Bretschneider, T., Schleicher, M., and Faix, J. (2005) Formins and VASPs may co-operate in the formation of filopodia. *Biochem. Soc. Trans.* **33,** 1256–1259
5. Vignjevic, D., Kojima, S., Aratyn, Y., Danciu, O., Svitkina, T., and Borisy, G. G. (2006) Role of fascin in filopodial protrusion. *J. Cell Biol.* **174,** 863–875
6. Mattila, P. K., Pykäläinen, A., Saarikangas, J., Paavilainen, V. O., Vihinen, H., Jokitalo, E., and Lappalainen, P. (2007) Missing-in-metastasis and IRSp53 deform PI(4,5)P2-rich membranes by an inverse BAR domain-like mechanism. *J. Cell Biol.* **176,** 953–964
7. Scita, G., Confalonieri, S., Lappalainen, P., and Suetsugu, S. (2008) IRSp53: crossing the road of membrane and actin dynamics in the formation of membrane protrusions. *Trends Cell Biol.* **18,** 52–60
8. Zhao, H., Pykäläinen, A., and Lappalainen, P. (2011) I-BAR domain proteins: linking actin and plasma membrane dynamics. *Curr. Opin. Cell Biol.* **23,** 14–21
9. Futó, K., Bódis, E., Machesky, L. M., Nyitrai, M., and Visegrády, B. (2013) Membrane binding properties of IRSp53-missing in metastasis domain (IMD) protein. *Biochim. Biophys. Acta* **1831,** 1651–1655
10. Yokouchi, M., Suzuki, R., Masuhara, M., Komiya, S., Inoue, A., and Yo-

shimura, A. (1997) Cloning and characterization of APS, an adaptor molecule containing PH and SH2 domains that is tyrosine phosphorylated upon B-cell receptor stimulation. *Oncogene* **15,** 7–15
11. Yousaf, N., Deng, Y., Kang, Y., and Riedel, H. (2001) Four PSM/SH2-B alternative splice variants and their differential roles in mitogenesis. *J. Biol. Chem.* **276,** 40940–40948
12. Iseki, M., Takaki, S., and Takatsu, K. (2000) Molecular cloning of the mouse APS as a member of the Lnk family adaptor proteins. *Biochem. Biophys. Res. Commun.* **272,** 45–54
13. Huang, X., Li, Y., Tanaka, K., Moore, K. G., and Hayashi, J. I. (1995) Cloning and characterization of Lnk, a signal transduction protein that links T-cell receptor activation signal to phospholipase Cγ1, Grb2, and phosphatidylinositol 3-kinase. *Proc. Natl. Acad. Sci. U.S.A.* **92,** 11618–11622
14. Nelms, K., O'Neill, T. J., Li, S., Hubbard, S. R., Gustafson, T. A., and Paul, W. E. (1999) Alternative splicing, gene localization, and binding of SH2-B to the insulin receptor kinase domain. *Mamm. Genome* **10,** 1160–1167
15. Chen, L., and Carter-Su, C. (2004) Adaptor protein SH2-Bβ undergoes nucleocytoplasmic shuttling: implications for nerve growth factor induction of neuronal differentiation. *Mol. Cell. Biol.* **24,** 3633–3647
16. Chen, L., Maures, T. J., Jin, H., Huo, J. S., Rabbani, S. A., Schwartz, J., and Carter-Su, C. (2008) SH2B1β (SH2-Bβ) enhances expression of a subset of nerve growth factor-regulated genes important for neuronal differentiation including genes encoding urokinase plasminogen activator receptor and matrix metalloproteinase 3/10. *Mol. Endocrinol.* **22,** 454–476
17. Maures, T. J., Chen, L., and Carter-Su, C. (2009) Nucleocytoplasmic shuttling of the adaptor protein SH2B1β (SH2-Bβ) is required for nerve growth factor (NGF)-dependent neurite outgrowth and enhancement of expression of a subset of NGF-responsive genes. *Mol. Endocrinol.* **23,** 1077–1091
18. Lin, W. F., Chen, C. J., Chang, Y. J., Chen, S. L., Chiu, I. M., and Chen, L. (2009) SH2B1β enhances fibroblast growth factor 1 (FGF1)-induced neurite outgrowth through MEK-ERK1/2-STAT3-Egr1 pathway. *Cell. Signal.* **21,** 1060–1072
19. Chang, Y. J., Chen, K. W., Chen, C. J., Lin, M. H., Sun, Y. J., Lee, J. L., Chiu, I. M., and Chen, L. (2014) SH2B1β interacts with STAT3 and enhances fibroblast growth factor 1-induced gene expression during neuronal differentiation. *Mol. Cell. Biol.* **34,** 1003–1019
20. Doche, M. E., Bochukova, E. G., Su, H. W., Pearce, L. R., Keogh, J. M., Henning, E., Cline, J. M., Saeed, S., Dale, A., Cheetham, T., Barroso, I., Argetsinger, L. S., O'Rahilly, S., Rui, L., Carter-Su, C., and Farooqi, I. S. (2012) Human SH2B1 mutations are associated with maladaptive behaviors and obesity. *J. Clin. Invest.* **122,** 4732–4736
21. Volckmar, A. L., Bolze, F., Jarick, I., Knoll, N., Scherag, A., Reinehr, T., Illig, T., Grallert, H., Wichmann, H. E., Wiegand, S., Biebermann, H., Krude, H., Fischer-Posovszky, P., Rief, W., Wabitsch, M., *et al.* (2012) Mutation screen in the GWAS derived obesity gene SH2B1 including functional analyses of detected variants. *BMC Med. Genomics* **5,** 65
22. Sandholt, C. H., Vestmar, M. A., Bille, D. S., Borglykke, A., Almind, K., Hansen, L., Sandbæk, A., Lauritzen, T., Witte, D., Jørgensen, T., Pedersen, O., and Hansen, T. (2011) Studies of metabolic phenotypic correlates of 15 obesity associated gene variants. *PLoS One* **6,** e23531
23. Rui, L., and Carter-Su, C. (1999) Identification of SH2-bβ as a potent cytoplasmic activator of the tyrosine kinase Janus kinase 2. *Proc. Natl. Acad. Sci. U.S.A.* **96,** 7172–7177
24. Qian, X., Riccio, A., Zhang, Y., and Ginty, D. D. (1998) Identification and characterization of novel substrates of Trk receptors in developing neurons. *Neuron* **21,** 1017–1029
25. Shih, C. H., Chen, C. J., and Chen, L. (2013) New function of the adaptor protein SH2B1 in brain-derived neurotrophic factor-induced neurite outgrowth. *PLoS One* **8,** e79619
26. Wang, T. C., Chiu, H., Chang, Y. J., Hsu, T. Y., Chiu, I. M., and Chen, L. (2011) The adaptor protein SH2B3 (Lnk) negatively regulates neurite outgrowth of PC12 cells and cortical neurons. *PLoS One* **6,** e26433
27. Rui, L., Mathews, L. S., Hotta, K., Gustafson, T. A., and Carter-Su, C. (1997) Identification of SH2-Bβ as a substrate of the tyrosine kinase JAK2 involved in growth hormone signaling. *Mol. Cell. Biol.* **17,** 6633–6644
28. Ho, S. Y., Chao, C. Y., Huang, H. L., Chiu, T. W., Charoenkwan, P., and Hwang, E. (2011) NeurphologyJ: an automatic neuronal morphology quantification method and its application in pharmacological discovery. *BMC Bioinformatics* **12,** 230
29. Bisi, S., Disanza, A., Malinverno, C., Frittoli, E., Palamidessi, A., and Scita, G. (2013) Membrane and actin dynamics interplay at lamellipodia leading edge. *Curr. Opin. Cell Biol.* **25,** 565–573
30. Disanza, A., Mantoani, S., Hertzog, M., Gerboth, S., Frittoli, E., Steffen, A., Berhoerster, K., Kreienkamp, H. J., Milanesi, F., Di Fiore, P. P., Ciliberto, A., Stradal, T. E., and Scita, G. (2006) Regulation of cell shape by Cdc42 is mediated by the synergic actin-bundling activity of the Eps8-IRSp53 complex. *Nat. Cell Biol.* **8,** 1337–1347
31. Diakonova, M., Helfer, E., Seveau, S., Swanson, J. A., Kocks, C., Rui, L., Carlier, M. F., and Carter-Su, C. (2007) Adaptor protein SH2-Bβ stimulates actin-based motility of *Listeria monocytogenes* in a vasodilator-stimulated phosphoprotein (VASP)-dependent fashion. *Infect. Immun.* **75,** 3581–3593
32. Yang, C., Hoelzle, M., Disanza, A., Scita, G., and Svitkina, T. (2009) Coordination of membrane and actin cytoskeleton dynamics during filopodia protrusion. *PLoS One* **4,** e5678
33. Maures, T. J., Su, H. W., Argetsinger, L. S., Grinstein, S., and Carter-Su, C. (2011) Phosphorylation controls a dual-function polybasic nuclear localization sequence in the adaptor protein SH2B1β to regulate its cellular function and distribution. *J. Cell Sci.* **124,** 1542–1552
34. Rider, L., Tao, J., Snyder, S., Brinley, B., Lu, J., and Diakonova, M. (2009) Adaptor protein SH2B1β cross-links actin filaments and regulates actin cytoskeleton. *Mol. Endocrinol.* **23,** 1065–1076
35. Vaggi, F., Disanza, A., Milanesi, F., Di Fiore, P. P., Menna, E., Matteoli, M., Gov, N. S., Scita, G., and Ciliberto, A. (2011) The Eps8/IRSp53/VASP network differentially controls actin capping and bundling in filopodia formation. *PLoS Comput. Biol.* **7,** e1002088
36. Funato, Y., Terabayashi, T., Suenaga, N., Seiki, M., Takenawa, T., and Miki, H. (2004) IRSp53/Eps8 complex is important for positive regulation of Rac and cancer cell motility/invasiveness. *Cancer Res.* **64,** 5237–5244